An Angularly and Spatially Resolved Reflectometer for a Perceptually Adequate Characterization of Gloss

Mikael Lindstrand†

STFI, Swedish Pulp and Paper Research Institute, Stockholm, SWEDEN

Gloss, as has long been known, is a far more complex visual concept than the present methods of instrumental gloss evaluation are able to characterize. The instrumental analyses are either highly oversimplified (standard gloss meters) or oversimplified but with results still difficult to interpret (goniophotometry). The dimensionality and power of the directed reflectance information measured by existing tools is lower and less expressive than the information gained from a direct visual examination of a surface. In this article, a new measurement principle for gloss characterization is presented, aimed to give more comprehensive gloss information, which at the same time has an intuitive interpretation. The integrated optical system is compact and has illumination and receptor devices in fixed positions, which facilitates a mechanically simple realization. The instrument is a goniophotometer with a spatial resolution, but it is restricted to a constant angle between the illumination and the receptor. The measurement yields a "Reflectance Vector Map" (RVM) which is an approximate optical equivalent to the surface measured. The RVM simultaneously contains spatially resolved information about directed reflectance and surface apparent inclination. The resolution is high in both spatial and in angular coordinates. The measurement provides a complex massive data set, which when appropriately visualized is similar to the visual properties of the original surface and thus encourages further evaluation and interpretation. A homogeneity index called "Gloss Angle Smoothness" (GAS) is introduced, derived from the RVM, by weighing perceptually "positive" and "negative" components of gloss. The index correlates well with results obtained by a panel of experienced gloss judges asked to rate gloss homogeneity for the limited but demanding set of black printed paper surfaces tested. The GAS index performs considerably better than a panel of inexperienced judges.

Journal of Imaging Science and Technology 49: 71–84 (2005)

Introduction

The perception and measurement of gloss are complicated concepts. There is a lack of clear and commonly accepted definition of gloss related to visual perception. Often is high gloss seen as an indication of high quality, e.g., in advertising prints. It is however questionable if high gloss as such is desirable. Another criterion may be to what degree it is possible to avoid irritating glare effects from a print. The topic of gloss in relation to perception, measurement and characterization is treated in some depth by the author in a review article.[1]

When measuring the directed reflectance from a paper surface, the maximum reflection is normally not obtained in the specular direction but at a slightly larger angle. This angular offset effect is well known and reported for both plain unprinted papers[2,3] as well as printed papers.[3–6] The difference in angle can be as much as 5-10 degrees and is hence important. This distinction is often neglected in the literature, but it is important when relating measured to observed gloss. Two definitions are given here. The first is adopted from ASTM, Standard Terminology of Appearance[7] and the second has been introduced previously[8] by the author. As indicated in Fig. 1:

- Specular angle (SA): the angle equal and opposite to the angle of incidence, i.e., SA = $-\alpha$.
- Peak angle (PA): the angle at which the directed reflection has its peak value.

An observer inspecting a surface under ordinary visual conditions is normally not aware about this distinction between SA and PA. The "specular behavior" is visually inspected under the direction of maximum reflectance, even if the SA and the PA are not equal. The distinction is however important when a surface is characterized instrumentally as a basis for predicting how the surface is perceived.

The aim of the present work is to present a measurement system which provides an objective description of the gloss from a surface, powerful enough to have the potential to yield results in concert with the results of perceptual evaluations. This has two implications. (i) It is necessary to adopt a multidimensional measurement approach. (ii) Although little may be gained, in any given application, by modeling the diffraction in the light-surface interaction on a local basis, the *effects* of the diffraction behavior of a surface are visible and hence have

Original manuscript received February 11, 2004

†Corresponding Author: M. Lindstrand, mikael.lindstrand@sca.com; Present address: SCA Graphic Research AB, Sundsuall, Sweden

Supplemental Material—An Appendix can be found on the IS&T website (www.imaging.org) for a period of no less than 2 years from the date of publication.

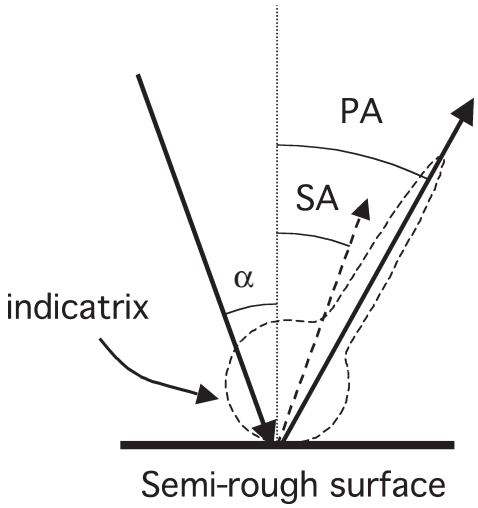

Figure 1. Illustration of Specular Angle (SA) and Peak Angle (PA) of a semi-micro-rough surface. The SA is equal but opposite to the angle of incidence (α). The directed reflectance may be considerably lower at the SA than at the PA.

to be incorporated in the model even if only with a phenomenological approach. Although the small-scale surface irregularities within a facet are not resolvable by the unaided eye, the surface appears matt due to such irregularities. Hence the directed reflectance (related to the degree of irregularities) of the facets should be characterized.

This work deals only with the geometric properties of reflectance. Chromatic effects are not measured. The aim of present work is not to give a complete physically based explanation of the reflectance characteristics. The Facet Map model forms the basis for the objective characterization of gloss, both spatially and angularly. The measurements lead to a "Reflectance Vector Map" (RVM), which on a surface element basis holds information about directed reflectance and surface apparent inclination. Multiple scattering and facet masking are not included in the model. However, as the directed reflectance characterization of each facet is closely correlated to the roughness and topography of the surface, an indirect dependence of the multiple scattering effects is recorded. If such effects are visible to the naked eye, then the system should also register the effects.

The RVM could be used for a wide range of applications. One example is for detailed studies of the directed reflectance behavior of the surface, e.g., in the context of perceptual evaluation studies.[8] Another application is given in the present work: to provide an objective measure of gloss homogeneity in concert with human visual perception. The Gloss Angle Smoothness (GAS) index, derived from the RVM, is here introduced as an objective estimate of the visually perceived gloss evenness of the surface. In principle each facet is ranked from positive to negative by a rating index in the range from +1 to –1, on the basis on its tilt. The rating index is multiplied by the reflectance of the facet to give a facet rating number, and the average for all facets of the sample surface is the Gloss Angle Smoothness index (GAS index).

This article has a background in a Master's Thesis work,[9] a Swedish[10] and a U.S. patent.[11]

The Measurement System

The measurement system, see Fig. 2, consists essentially of a cylindrical sample holder controlled by a stepping motor, a CCD camera, an illumination device, an image capture device and a computer. The reflectance from the surface is recorded by the camera, between intermittent periodic sample-holder rotations.

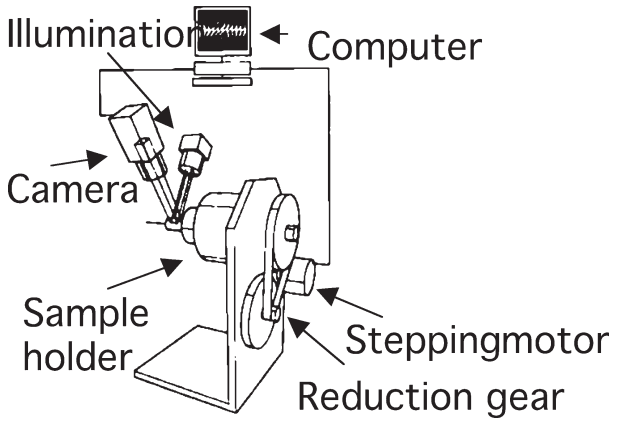

Figure 2. Sketch of the system. Overall height from the bottom of the sample holder support to the top of the camera is appx. 400 mm.

General Description

The cylindrical sample holder device is a high-precision instrument in itself. The radius used in this study is 8.0 mm. The rotation of the holder is controlled by a stepping motor (6000 steps/rev.) via a reduction gear resulting in a theoretical resolution of appx. 2.8×10^5 steps/rev. or 1.3×10^{-3} degrees/step. It is necessary to have a high accuracy in the overall positioning of the sample holder although this extreme rotation resolution has been shown to be exaggerated. The resolution necessary is a function of the set-up as a whole but with given specifications a resolution of appx. 5000 steps/rev. would be sufficient. The rotation of the sample holder is computer controlled.

The camera and illumination devices, see Fig. 3, are identical to those presented in similar studies[12–14] but a short description of the characteristics are given below. Although one of the characteristics of the present work is the curved sample holder, the sample surface in Fig. 3 is flat in order to simplify the ray-tracing illustration to characterize the optics. The detector system is a charged couple device (CCD) video camera with a spatial resolution of 512×512 pixels and an 8-bit dynamic resolution. The response of the camera is close to linear in the dominating range (appx. from gray level 10 to 255) of its operating range (0–255). However in the low intensity region (corresponding to gray scale up to appx. 7) the data output diverts for the linear relationship. The illumination has a white incandescent light source and collimating optics (75 mm, f/1.4 lens, illumination sector appx. 2°) to yield a converging beam covering an area larger than the field of view of the camera. Both the camera and the illumination are set at an angle of 20° to the normal to the sample surface. In this work, the limited dynamic range of the CCD has been utilized in an effective manner by tuning the illumination to each sample individually. The drawback is naturally that no mean gloss level can be measured or calculated. The camera objective (60 mm, f/11 lens, acceptance angle appx. 1°) is adjusted to give a field of view of appx. 10.0 mm × 10.6 mm for a flat mounted sample surface. The non-quadratic field of view is a consequence of the pro-

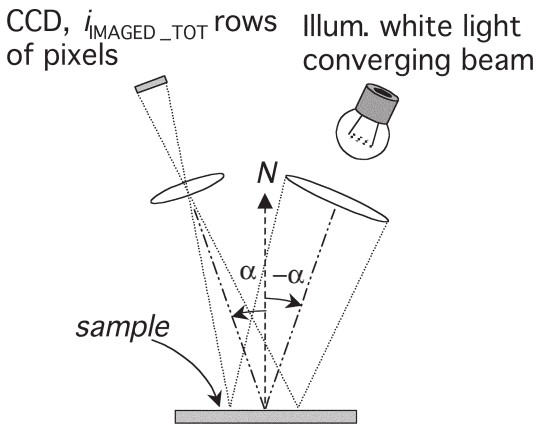

Figure 3. The Illumination-Camera set up. The optics on the illumination side yields a converging beam.

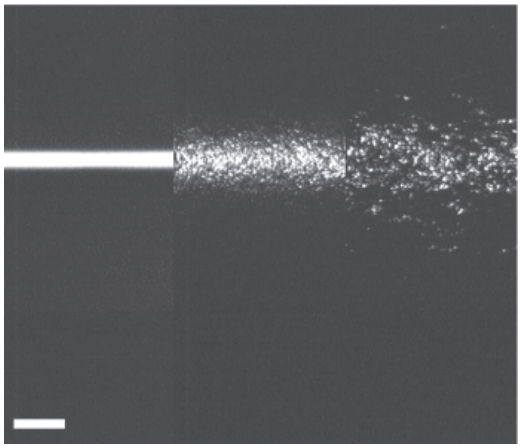

(a) (b) (c)

Figure 4. Three different samples mounted on the sample holder in Fig. 2. The inset bar in the lower left corner corresponds to 1 millimeter. (a) A very smooth black plastic film (photographic negative). (b) A black printed paper, considered to be a high gloss quality paper with a low degree of gloss inhomogeneity. The paper is a woodfree, clay-coated (20 g/m^2) paper printed in a sheet offset press 400 percent black, i.e., 100 percent of each process color. (c) A black printed paper, considered to be a be a low quality paper with a high degree of gloss inhomogeneity. The paper is a light weight coated (LWC) paper printed in a heat set web offset press. The measurement is made across the machine direction (the machine direction is horizontally orientated in this image). This sample was cut directly from a magazine so no further information is available.

jection of a flat sample surface onto the camera having an inclination (10/cos20° ≈ 10.6). The camera output is fed via a frame grabber to a computer for analysis.

Angularly and Spatially Resolved Reflectometry

For gloss measurements in general, even a very small deviation in the positioning of the sample surface, the illumination or the receptor can have a large impact on the results of a measurement. The position of a rigid body has six degrees of freedom, described by its position on the *x*-, *y*-, and *z*-axes together with the three rotational dimensions around these axes. Care must therefore be taken to ensure that these six parameters for the sample, the illumination and the receptor are well tuned during the measurement session.

The sample is mounted on a cylindrical holder. In the present work the sample has been fixed with adhesive tape, which means that the borders (appx. 2-3 mm. on each edge) of the sample are destroyed. Except for these small areas, the test procedure is very kind to the sample and the same region can if desired be re-measured many times, and the surface can subsequently be tested in other measurement equipment.

When a smooth and glossy sample is viewed on a cylindrical holder, see Fig. 4(a), we see a narrow zone of strongly reflecting surface, quickly declining on each side of this zone in the curved direction. In the glossy zone the surface is positioned ideally with respect to level of observed local reflectance, and we have a local specular reflectance, but on each side of the specular reflectance zone, the inclination of the sample is not ideal with respect to the level of observed local reflectance and the observed directed reflectance decreases. For surfaces with a higher degree of topographic variation, however, the glossy zone is not distinct, see Fig. 4(b) and Fig. 4(c). Local glare effects can be observed in otherwise dark regions. Surface undulations, leads to reflectance undulation when viewing is in one same direction. In the glare positions, the local angle of the surface is opposite to the local angle of the curved sample holder. The two local angles cancel each other out and the surface is ideally positioned with respect to the level of observed local reflectance, see Fig. 5. The described dependence between a position on the sample holder, the rotation of the sample holder and the local inclination which it enforces on the sample surface is one of the main features of this measurement device. It makes it possible to accurately control and perform measurements with different local inclinations for the sample and at the same time keep track of and thereby relate these multiple measurements to exact physical positions on the sample surface. In other words, for a fixed set-up of illumination and detection (camera): there will be a change in the intensity of light reflected from any given spot on the sample, as the inclination of the sample is changed. The reflectance is measured for a large number of different inclinations during the rotation of the sample. The core of the measurement is thus to measure, analyze and characterize the directed reflectance of each local facet as a function of the sample inclination.

The information obtained thus represents a three-dimensional volume, see Fig. 6, where the *x*- and *y*-coordinates of the information volume correspond to the *x*- and *y*-coordinates in the sample surface, and the *z*-coordinate corresponds to the inclination of local area on the sample holder and the stored voxel value, i.e., f(*x,y,z*) is the measured reflectance value for that sample position at a given inclination.

The Reflectance Vector Map (RVM)

In the present implementation, the measured data is greatly reduced. For each (*x,y*)-position, only the maximum reflectance value and the corresponding sample holder inclination value are stored. This maximum reflectance value is assigned as the "directed reflectance" of the facet, and the inclination of the sample holder is assigned as the "tilt" of the facet. The sign of the tilt is however reversed, as the surface and the sample holder have opposite inclinations when the maximal reflectance is recorded. The "tilt" information of the RVM, is synonymous to the expression "apparent inclination" of the facet, meaning the aggregate information of the angle of a facet plane in proximity to the physical surface, together with the angle offset of the optical effect which

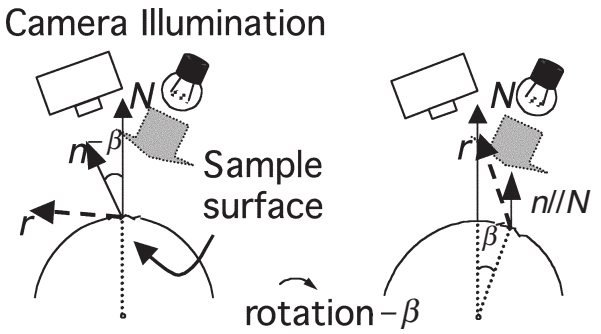

Figure 5. Illustration of the relationship between the rotation of the sample holder and the local inclination of the sample. *N* is the normal to the top of the sample holder itself, *n* is the local normal to a specific facet of interest, *r* is the peak reflection direction from that same facet. Rotating the sample holder $-\beta$ degrees corresponds to an enforced inclination change of the sample surface of $-\beta$ degrees.

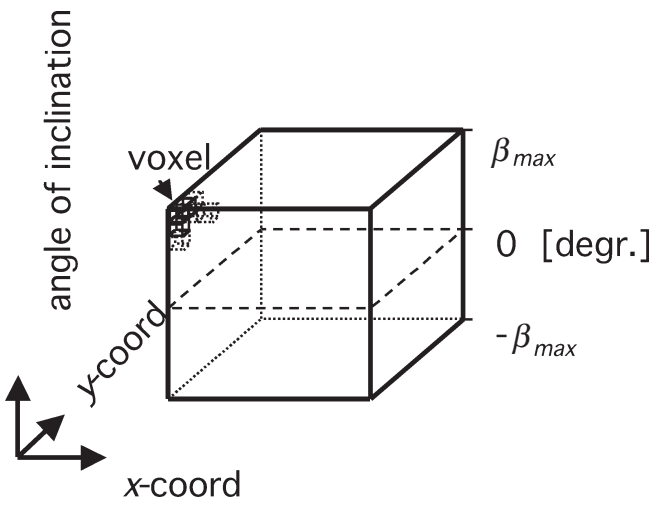

Figure 6. Three-dimensional representation of the reflectance information scanned during a measurement session. A smooth plastic film would have a very pronounced intensity peak at and near the plane where the "angle of inclination" equals 0 (zero) degrees. A rough surface with a high degree of gloss inhomogeneity would have local high intensities far off the plane where the "angle of inclination" equals 0 degrees.

the surface roughness has on the reflection. The term "tilt" will in present work be used only in the context of the apparent angular inclination of a facet relative to the global surface normal.

The reason for the data reduction is not that the omitted data is of no interest, but the condensation of the measurement data from a large reflection volume into a much more compact form still yields an information-set of high explanatory power dealing with multiple aspects of the gloss characteristics of importance to a human judge. The result after this data reduction is here called the "Reflectance Vector Map" (RVM).

The RVM carries information of the *Directed reflectance* and *Tilt*, and is thereby an approximate optical equivalent to the real surface under certain limitations. The approximation involves certain limitations in resolution, and the observation is restricted to only one angular plane, c.f. mono-plane goniophotometry.

"Gloss Angle Smoothness" GAS

Starting by one single facet, it could on its own merits be judged in terms of how perceptually pleasing it appears, in terms of visual gloss. The following principally different cases for the appearance of a facet can be stated. A facet can be judged as:

1) **Very good:** high reflectance and a low directional deviation from the overall PA, i.e., the facet contributes to the directed reflectance in the PA.
2) **Good:** moderate reflectance and a low directional deviation from the overall PA.
3) **Poor:** moderate reflectance and a non-negligible directional deviation from the overall PA.
4) **Very poor:** high reflectance and a non-negligible directional deviation from the overall PA.

In the implementation, there is, of course, a continuous transition from very good to very poor. The first two examples are "positive" facets, whereas the last two are "negative" facets. Category 4) is perceptually most disturbing. This type of surface region is responsible for the poor print quality recorded when the observer has to incline the sample through a large angle to eliminate disturbing "glare" and "glitter" effects. These, and category 3) regions may also reduce densitometry values, i.e., black regions appear grayer (less black) and color regions less saturated.

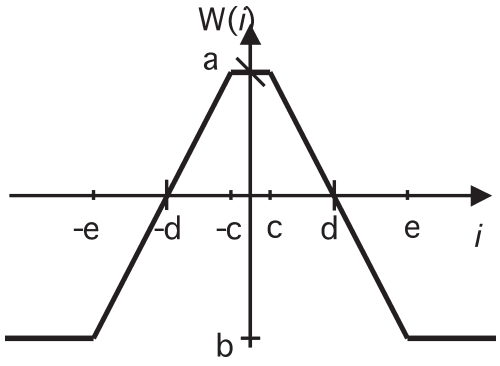

Figure 7. The weighting function for rating a facet to be "positive" or "negative", in terms of estimated perceptual gloss quality. The variable *i* represents row index in present implementation: a = 1, b = –1, c = 2, d = 8 and e = 14 (overdetermined specifications here for the convenience of the reader).

Since the weighting function operates on facet angles in relation to PA and not SA, the optical off-specular reflection effect of surface roughness is cancelled out, and reflection inhomogeneities are judged relative to the PA. The weighting function used, see Fig. 7, rates each facet in the range, arbitrarily chosen to be from $b = -1$ to $a = +1$ as a function of the tilt inclination i. The weighting function can be seen as a non-crisp rule in a fuzzy rule base.

The Test Sample Set

The sample set, chosen to provide sufficient variation in the evaluation results to make it possible to draw enlightening conclusions, consisted of seven blade-coated specimens with the same base paper. The coatings differed both in composition and in amount, see Table I. The base paper was a 63 g/m^2 "woodfree" calendered paper. Two different coating pigments were used, calcium

TABLE I. Sample Description

Sample	Coating pigment	Coat Weight [g/m²]	Gloss 75° (Hunter)
s11	Kaolin	20	92.6
s10	Kaolin	15	87.1
s12	Kaolin	11	85.8
s24	$CaCO_3$	19	81.3
s23	$CaCO_3$	15	77.4
s26	$CaCO_3$	11	72.3
s25	$CaCO_3$	7	56.2

carbonate and Kaolin with coat weights in the ranges 7 – 19 g/m² and 11 – 20 g/m² respectively, see Table I. All specimens were printed in sheet-fed offset at 400 percent, i.e., 100% each of cyan, magenta, yellow and black.

Perceptual Evaluation

The perceptual evaluation panel consisted of 11 judges, with normal or corrected-to-normal vision. Six of the judges were considered to have a long experience in visual gloss evaluation. They had all worked on gloss related issues for at least several months, some of them for well over ten years. The other five had no previous experience of the perceptual evaluation of gloss. The panel of judges evaluated some dummy samples before starting the perceptual evaluation of the "gloss inhomogeneity" of the samples. The subjects were encouraged both to incline the samples in different directions and to curve the samples into a convex shape during the evaluation, all to facilitate the visual evaluation process. The subjects were asked to rank the samples from "1" (the best, with the lowest degree of inhomogeneity) to "7" (the worst).

Implementation of the Measurement Algorithm

The curved sample holder means that there is a continuous non-linear change in sample holder inclination, β, relative to the illumination-camera set-up and as a function of row index in the CCD-camera, i_{IMAGED}, as indicated in Fig. 5 and Fig. 8. The angle $\beta(i_{\text{IMAGED}})$ is defined relative to the bisector of the optical axes of the camera and the illumination. This functional dependence between row index and inclination must be analytically expressed in order to enable the local tilt of each facet to be assessed during the measurement session. The angle-position dependence, $\beta(i_{\text{IMAGED}})$, is derived as follows.

The Inclination as a Function of Position on the Sample Holder

Important parameters (see Fig. 8) are: the radius of the sample holder, r, [in this implementation: 8.0 mm], the side length of the imaged area L_{IMAGED} [10.0 mm] and the inclination of the CCD relative to the bisector of the optical axes of the camera and the illumination α [20°]. The position of the point G is defined as the position of maximum reflectance for an optically smooth material, this position can be used for calibration of the system. Using a smooth and glossy reference material, e.g., the metallic sample holder itself, and by moving (translating, not rotating) the whole cylindrical holder relative to be camera/illumination-setup, the position G can be tuned to any desirable position. G was chosen to conform (fine-tuned and exactly) to CCD row index, i_{GLOSS} = 116, see motivation in the appendix.

To define an analytical expression for the inclination as a function of the position on the sample holder, the distance, L_1, from the CCD index 0 to G is given by

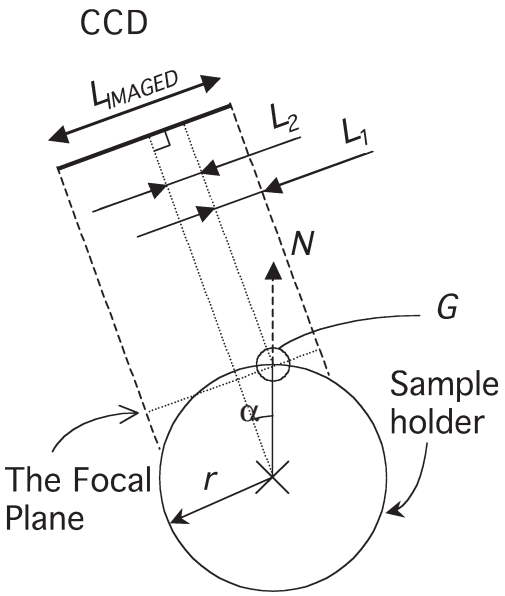

Figure 8. Sketch of the sample holder and some related variables. N is the normal to the sample holder at the bisector of the axis of the illumination and the axis of the camera. G is the point at which the gloss peak would appear for an optically smooth material. L_{IMAGED} is the side length of the imaged area measured as a plane parallel to the camera CCD. L_1 is the distance from the start of the imaged area (pixel row 0) to the point G. L_2 is the distance from the point G to the line parallel to the optical axis of the camera and coinciding with the axis of curvature of the sample holder.

$$L_1 = i_{\text{GLOSS}} \frac{L_{\text{IMAGED}}}{i_{\text{IMAGED\_TOT}}} \tag{1}$$

where $i_{\text{IMAGED\_TOT}}$ is the total number of rows in the CCD [512 pixel rows]. The distance, L_2, from G to the line parallel to the optical axis of the CCD coinciding with the center axis of the sample holder is:

$$L_2 = r \sin\alpha \tag{2}$$

The local angle of inclination β of the sample holder, relative to the normal N to the sample holder at position G, can be expressed as a function of the row index i_{IMAGED} at the CCD:

$$\beta(i_{\text{IMAGED}}) = \arcsin\left(\frac{L_1 + L_2 - i_{\text{IMAGED}} \dfrac{L_{\text{IMAGED}}}{i_{\text{IMAGED\_TOT}}}}{r}\right) - \alpha. \tag{3}$$

Combining Eqs. (2), (3) and (4), we can calculate the maximal inclination $\beta_{\max}$ on the sample holder for the current set-up:

$$\begin{aligned}\beta_{\max} &= \beta\big|_{i_{\text{IMAGED}}=0} = \arcsin\left(\frac{L_1 + L_2}{r}\right) - \alpha \\ &= \arcsin\left(\frac{i_{\text{GLOSS}} \dfrac{L_{\text{IMAGED}}}{i_{\text{IMAGED\_TOT}}} + r\sin\alpha}{r}\right) - \alpha\end{aligned} \tag{4}$$

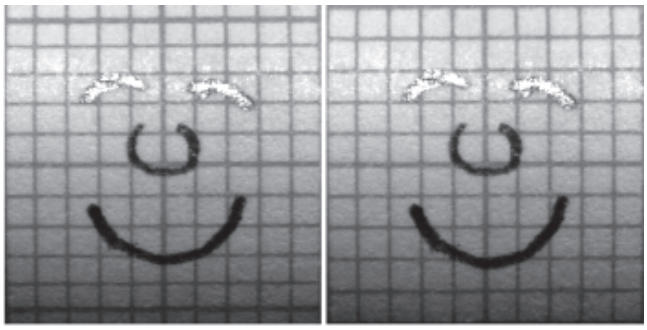

(a) (b)

Figure 9. (a) A photograph of a paper with a millimeter grid and a lead pencil sketch mounted on the sample holder in Fig. 2. The cylindrical shape causes the millimeter grid to appear spatially compressed mainly at the upper and lower borders in the image. (b) The image spatially retransformed from a nonlinear metric into the Cartesian metric.

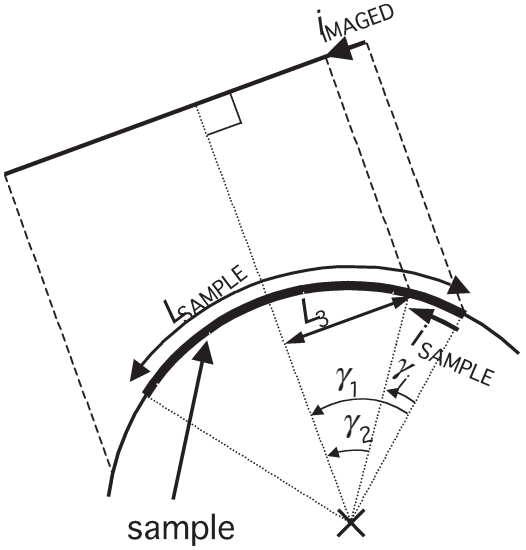

Figure 10. Detailed sketch of the sample holder and some related variables. i_{IMAGED} is an index in the pixel coordinate system of the camera image. L_{SAMPLE} is the side length of the sample surface. i_{SAMPLE} is an index in the facet coordinate system of the surface. L_3 is the distance from the line parallel to the optical axis of the camera and coinciding with the center of the sample holder to the point corresponding to i_{SAMPLE}. γ_1 is the angle defined by the radius coinciding the start of the imaged area and the radius parallel to the optical axis of the camera. γ_2 equals the angle defined by the radius at a point corresponding to i_{SAMPLE} and the radius parallel to the optical axis of the camera. $\gamma_i = \gamma_1 - \gamma_2$.

The maximal possible inclination is not symmetrical, since it is possible to enforce a larger local inclination of the sample towards the camera than towards the illuminator. Nevertheless β_{max} represents the maximal possible inclination in both directions around G. In the present set-up ($i_{GLOSS} = 116$, $L_{IMAGED} = 10.0$ mm., i_{IMAGED_TOT} = 512 pixel rows, r = 8 mm. and α = 20 degrees), the maximal possible angle that can be resolved in both directions is 18.7 degrees. This dynamic range of angles seems to be sufficient for printed paper surfaces in general, as a really pathologic paper example with swollen fibers and consequently a very disturbing gloss characteristic, showed angles only slightly larger than 10 degrees. For unprinted paper surfaces, however, the dynamic range is questionable. For one of the surfaces measured, the "Maple Leaf" sample, the histogram in Fig. 11(d) of the facet tilt shows that the angle range is insufficient.

The Transformation of the Camera Input to a Cartesian Metric

As the sample surface is mounted on a cylindrical sample holder and the image of the surface is projected onto a flat camera chip, there will be a transformation of metrics, i.e., physical distances in the sample surfaces will appear to be different when viewed in the camera, see Fig. 9(a). This change in metrics must be compensated for when mapping physical positions in the sample surface. The camera image of the sample is therefore transformed to a Cartesian metric; so that the image is uniformly flat although the image is recorded over a curved surface, see Fig. 9(b). This transformation is $i_{IMAGED} = f(i_{SAMPLE})$, where i_{IMAGED} is the coordinate system of the camera image, i.e., the curved sample as it appears when projected onto the flat CCD camera and i_{SAMPLE} is the coordinate system for the physical sample. The function can be derived as follows, see also Fig. 10. The angle γ_i subtended by an arc of length i_{SAMPLE} rows on the sample holder is given by:

$$\gamma_i = \frac{i_{SAMPLE}}{i_{SAMPLE\_TOT}} \frac{L_{SAMPLE}}{r} \frac{180}{\pi} \quad \text{[degrees]} \tag{5}$$

where i_{SAMPLE_TOT} is the number of facets of the sample (512), L_{SAMPLE} is the side length of the sample surface (10.0 mm), (r and i_{SAMPLE} as previous definitions). Based on Fig. 8, Fig. 10 and the previous derivation of β_{max}, the following relation can be stated:

$$\gamma_1 = \beta_{max} + \alpha \quad \text{[degrees]}. \tag{6}$$

Then, Fig. 10 gives:

$$\gamma_2 = \gamma_1 - \gamma_i = \beta_{max} + \alpha - \gamma_i \tag{7}$$

where γ_2 is the angle defined by the line parallel to the optical axis of the CCD coinciding with the center axis of the sample holder and the radius at position i_{SAMPLE} (α as previous definition). The distance L_3 from position i_{SAMPLE} to the optical axis is

$$L_3 = r \sin \gamma_2. \tag{8}$$

Then Figs. 8 and 10 gives:

$$i_{IMAGED} \frac{L_{IMAGED}}{i_{IMAGED\_TOT}} + L_3 = L_1 + L_2 \tag{9}$$

which trivially can be rearranged into

$$i_{IMAGED} = \frac{i_{IMAGED\_TOT}}{L_{IMAGED}} (L_1 + L_2 - L_3). \tag{10}$$

The transformation $i_{IMAGED} = f(i_{SAMPLE})$ can be calculated, based on Eq. (11). By first combining Eqs. (2), (3) and (9), then using Eq. (8), then Eq. (5) and finally Eq. (6), an explicit expression of the transformation is obtained, see Eq. (11).

$$
\begin{aligned}
i_{\mathrm{IMAGED}} = \mathrm{f}(i_{\mathrm{SAMPLE}}) &= \frac{i_{\mathrm{IMAGED\_TOT}}}{L_{\mathrm{IMAGED}}}\left(i_{\mathrm{GLOSS}}\frac{L_{\mathrm{IMAGED}}}{i_{\mathrm{IMAGED\_TOT}}} + r\sin\alpha - r\sin\gamma_2\right) = \\
&= i_{\mathrm{GLOSS}} + \frac{i_{\mathrm{IMAGED\_TOT}}r}{L_{\mathrm{IMAGED}}}\left(\sin\alpha - \sin\left(\beta_{\max} + \alpha - \gamma_i\right)\right) = \\
&= i_{\mathrm{GLOSS}} + \frac{i_{\mathrm{IMAGED\_TOT}}r}{L_{\mathrm{IMAGED}}}\left(\sin\alpha - \sin\left(\arcsin\left(\frac{i_{\mathrm{GLOSS}}\dfrac{L_{\mathrm{IMAGED}}}{i_{\mathrm{IMAGED\_TOT}}} + r\sin\alpha}{r}\right) - \alpha + \alpha - \gamma_i\right)\right) \\
&= i_{\mathrm{GLOSS}} + \frac{i_{\mathrm{IMAGED\_TOT}}r}{L_{\mathrm{IMAGED}}}\left(\sin\alpha - \sin\left(\arcsin\left(\frac{i_{\mathrm{GLOSS}}\dfrac{L_{\mathrm{IMAGED}}}{i_{\mathrm{IMAGED\_TOT}}} + r\sin\alpha}{r}\right) - \frac{i_{\mathrm{SAMPLE}}}{i_{\mathrm{SAMPLE\_TOT}}}\frac{L_{\mathrm{SAMPLE}}}{r}\frac{180}{\pi}\right)\right).
\end{aligned}
\tag{11}
$$

Since this transformation is only one-dimensional and is static, a transformation vector can be calculated once at the beginning of the measurement. This vector can then be used as a look-up table throughout the measurement session. In this implementation no interpolation of sample data is performed in the transformation, the sample row closest to the desired position according to Eq. (11) is chosen. A measurement is performed with the sample holder in a large number of different positions. Each time, the sample holder is rotated through an angular increment, an image is taken, the metric transformation is performed and a lateral translation is introduced to move the reflectance information through the distance through which the sample was incrementally rotated. A large number of images are thus obtained. The images differ in that the reflectance is recorded for different local inclinations. The full scan of the 3D volume in Fig. 5 is thus obtained.

In the present implementation the whole volume data is scanned but it is not stored. Instead, the data is compressed into the RVM as described earlier.

The GAS Implemented

The parameters were chosen to yield a balanced output of positively and negatively rated facets for a wide range of printed test samples. That is, the parameters were chosen, based on a range of different surfaces other than the surfaces in this study, made before the present evaluation. If the positive zone of the weighting function is too narrow or too wide, the ability of the system to distinguish similar samples will become poor. The input range for which the weighting function has a positive output, appx. $|i| \le 1.2°$ ($c \approx 0.30°$, $d \approx 1.2°$ and $d \approx 2.1°$), may still appear narrow. As the parameters of the weight function is closely related to the RVM, the RVM is a topography characterization of the sample and as every topography characterization is partly a function of the characterization instrument itself, the weight function parameters are chosen given the spatial resolution of the RVM. In the present set up the RVM facet length was 20 μm. A coarser spatial resolution (larger facets) would low pass filter the surface topography, indicating a smoother surface with lower facet tilt for the same physical surface measured. The measurement system used is designed to resemble the human visual system in terms of spatial resolution. It has been reported[15] that imperfections of fractions of a degree are easily noticeable defects, but this referred to reflected images from a black polished glass. For a rougher paper surface, the visual system is less sensitive to surface imperfections. The chosen narrow range of positive output of the weighting function nevertheless yields positively rated facets, which outnumber the negatively rated with a margin, for all the paper surfaces tested.

The implemented version of the weighting function involves an approximation: it is a linear function of the pixel distance from the pixel row corresponding to the PA direction for the surface measured. The inclination index i in Fig. 6 can thus be changed to a row index i. Further details are given in the Appendix. The error is so small that it is considered to be negligible.

The rating value, $W(i)$ is multiplied by the local reflectance value to yield a local gloss "smoothness" rating value for the facet, in the range $-a$ to a, where a corresponds to 255 in the present implementation using 8-bit resolution of the value of reflectance. The mean value over all the facets is calculated. The smoothness values are then finally scaled to the range of 0 to b, where b was in the present implementation arbitrarily chosen to be 100. To sum up, the Gloss Angle Smoothness (GAS) index is calculated as:

$$
\mathrm{GAS} = \frac{b}{2a}\left(a + \frac{1}{mn}\sum_{i=1}^{m}\sum_{j=1}^{n}\left(\mathrm{RVM_R}(i,j)\times W\left(\mathrm{RVM_A}(i,j)\right)\right)\right), \tag{12}
$$

where m and n are the number of facets in the x and y directions, respectively, $\mathrm{RVM_R}$ represents the reflectance information, $\mathrm{RVM_A}$ represents the angle information and the operator "×" is an element (point)-wise multiplication operator.

Results

The Reflection Vector Maps (RVMs), are here illustrated as pairs of images, where the first represents the spatially resolved directed reflectance information and the second represents the spatially resolved tilt information, as shown in Fig. 11. The dimensions of the images are 10 × 10 mm.

Figure 11(a) illustrates the RVM for a fully exposed black plastic photographic film. The reflection map indicates a small but perceivable undulation. The undula-

TABLE II. Results and Statistics of the GAS Evaluation

	GAS-evaluation			Identical areas			Partly different areas		
Sample	1st	2nd	3rd	mean	std	95-conf	mean	std	95-conf
s11	71.5	71.3	72.8	71.4	0.14	0.20	71.9	0.81	0.92
s10	69.2	69.2	69.5	69.2	0.00	0.00	69.3	0.17	0.20
s12	68.0	68.0	68.8	68.0	0.00	0.00	68.3	0.46	0.52
s24	64.8	64.7	64.0	64.8	0.07	0.10	64.5	0.44	0.49
s23	60.1	60.2	60.0	60.2	0.07	0.10	60.1	0.10	0.11
s26	56.6	56.8	56.0	56.7	0.14	0.20	56.5	0.42	0.47
s25	47.1	47.1	45.9	47.1	0.00	0.00	46.7	0.69	0.78

In the 1st and 2nd GAS-evaluation, identical areas were measured. The statistics are presented under the column heading "Identical areas". For the 3rd GAS-evaluation, the samples were temporarily removed from the equipment and hence partly different areas are measured. The statistics are presented under the column heading "Partly different areas".

tion is more clearly visible in the Reflection map than in a direct inspection of the plastic film, where the reflectance undulation is hardly perceivable. The angle map illustrates how very smooth the photographic film is, with angles well within the range of [–0.6, 0.6] degrees.

Figure 11(b) illustrates the RVM for a printed paper, considered to have high degree of gloss homogeneity. The base paper was wood free, blade clay coated (~20 g/m^2) and printed (400%) in a sheet fed offset press.

Figure 11(c) illustrates the RVM for a heat-set offset printed Light Weight Coated (LWC) paper, considered by experienced visual gloss judges is to have an extremely poor gloss quality.

In Figs. 11(b) and 11(c) the range of angles was fixed at (–4, 4) degrees, to make comparisons between these two papers easier. A drawback is that the angle information for a number of facets is saturated, i.e., outside (–4, 4) degrees. The range of angles is however normally algorithmically adapted to the sample measured, and this makes a more detailed study feasible.

Figure 11(d) shows the RVM for a plain uncoated wood free paper with small electrophotograpically toner printed (an ordinary office laser printer) areas shaped like maple leaves, where these imaged areas are made glossy by applied local heat in combination with some degree of pressure, i.e., toner fusing.

Histograms of the facet tilts of selected areas of the "Maple Leaf"-sample, Fig. 11(d), may be drawn. Figure 12(a) illustrates masking positions for the tilt information of the "Maple Leaf" sample. The masking is used to select plain paper areas, black boxes in Fig. 12(a), and imaged areas, white boxes. In Fig. 12(b) the angle histogram for the whole 10 mm × 10 mm. "Maple Leaf" sample surface is depicted. In Fig. 12(c) the angle histogram for the imaged areas, white mask boxes in Fig. 12(a), is given and in Fig. 12(d) the angle histogram for the plain paper area, black mask boxes in Fig. 12(a).

TABLE III. Results of the Visual Assessment

	Judges										
Sample	E1	E2	E3	E4	E5	E6	N7	N8	N9	N10	N11
s11	1	1	1	1	1	1	5	7	6	6	5
s10	4	5	4	3	2	2	4	6	3	5	4
s12	5	3	3	2	4	3	3	2	7	3	3
s24	3	2	2	4	3	4	1	1	1	1	1
s23	2	4	5	5	5	5	2	3	2	4	2
s26	6	6	6	6	6	6	7	4	5	7	6
s25	7	7	7	7	7	7	6	5	4	2	7

The letters "E" and "N" before the judge number represent "Experienced" and "Novice" respectively.

The GAS Results

The GAS index for each of the seven samples is presented in Table II. Table III presents the results of the perceptual evaluation. The prefixes E and N denote "Experienced" and "Novice" judges respectively. Table IV presents the means, standard deviations and 95% confidence intervals for all judges, for the Experienced sub-group and for the Novice sub-group. Figure 13 shows the results for the Novice sub-group plotted against the results of the Experienced sub-group. The error bars represent the 95% confidence intervals. The coefficient of determination for the whole set, $r^2 \approx 0.02$.

The GAS Results in Relation to the Results of the Visual Evaluation

The performance of the GAS index algorithm was informaevaluated by relating the GAS index to the results of the perceptual evaluation. In Fig. 14, the GAS-evaluation results are plotted against the results of the perceptual evaluation for the Experienced sub-group. The error bars represent the 95% confidence intervals. The results and error bars for the GAS evaluation relate to measurements at different positions for each

TABLE IV. Statistics of Judgement Results

	All judges			Experienced sub-group			Novice sub-group		
Sample	mean	std	95-conf	mean	std	95-conf	mean	std	95-conf
s11	3.18	2.56	1.51	1.00	0.00	0.00	5.80	0.84	0.73
s10	3.82	1.25	0.74	3.33	1.21	0.97	4.40	1.14	1.00
s12	3.45	1.44	0.85	3.33	1.03	0.83	3.60	1.95	1.71
s24	2.09	1.22	0.72	3.00	0.89	0.72	1.00	0.00	0.00
s23	3.55	1.37	0.81	4.33	1.21	0.97	2.60	0.89	0.78
s26	5.91	0.83	0.49	6.00	0.00	0.00	5.80	1.30	1.14
s25	6.00	1.67	0.99	7.00	0.00	0.00	4.80	1.92	1.69

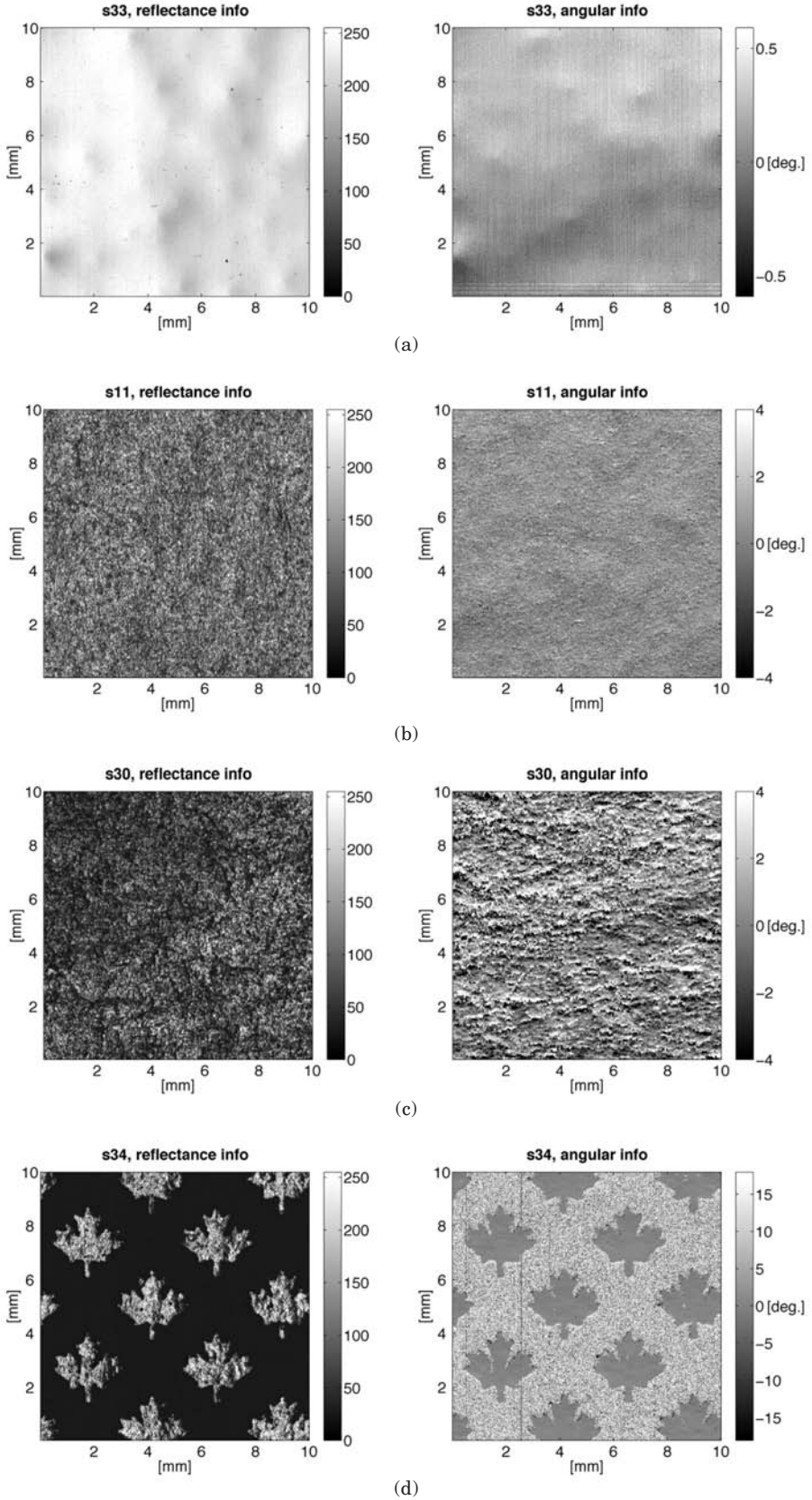

Figure 11. Reflectance vector maps (RVM) for four different samples. The RVM's are represented as pair-images, the left-hand column illustrates the reflectance information (arbitrary scale), and the right-hand column represents the angular information (degrees). Note that there are three different scales of angles. (a), (b) and (c) correspond to the samples in Fig. 4, numbered from left to right. (d) is an ordinary unprinted white office paper with small black imaged areas (maple leafs) printed in a laser printer. The imaged areas were subsequently treated with heat in combination with some degree of pressure in order to make the imaged areas glossy.

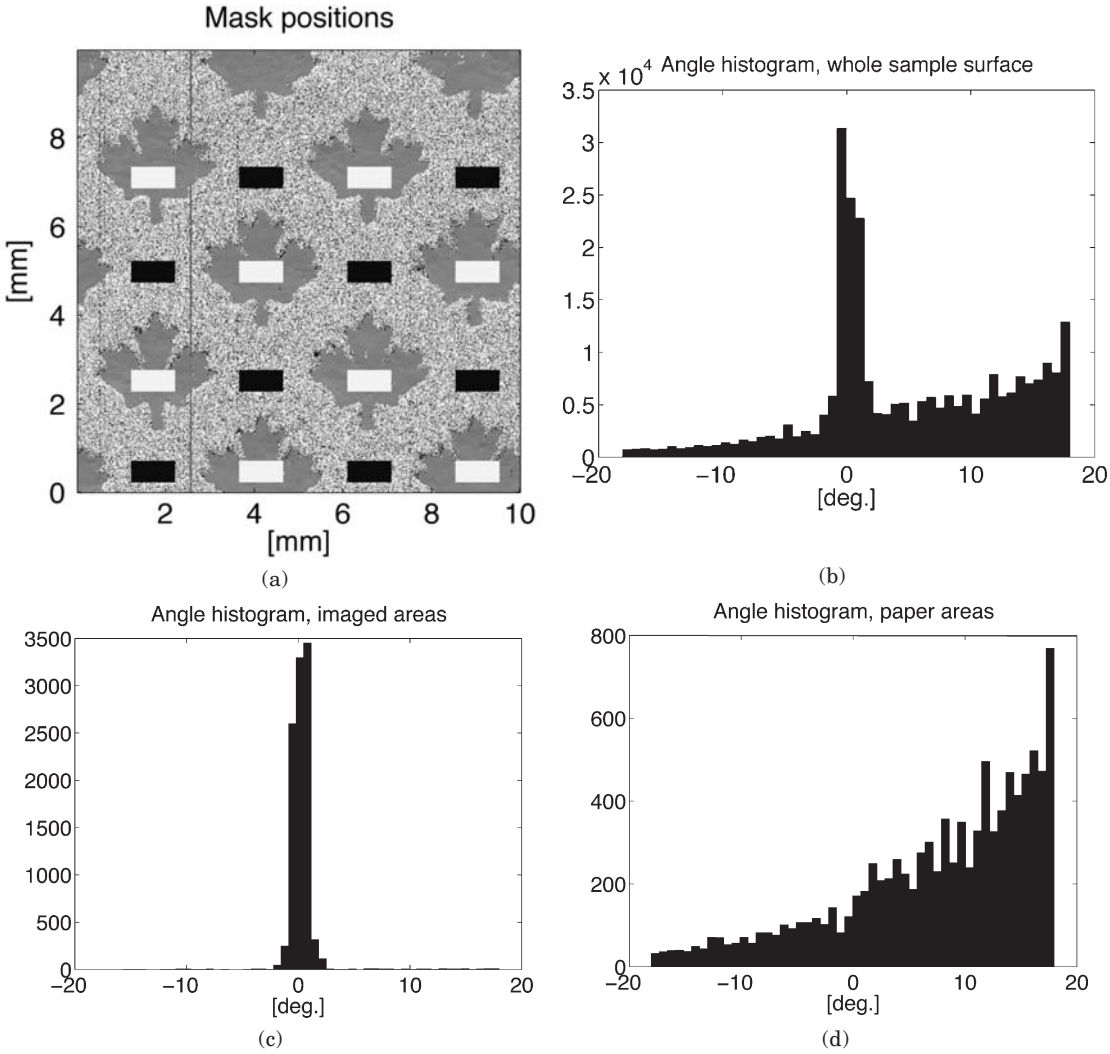

Figure 12. (a) Mask to separate imaged and unimaged (plain paper) areas on the sample. The white rectangles selects the imaged areas and the black rectangles selects the unimaged areas. (b) Histogram of the angle information of the whole surface, both imaged and unimaged surfaces. (c) Histogram of the angle information of the imaged areas, using the areas corresponding to the white rectangles in the mask in (a). (d) Histogram of the angle information of the unimaged areas, using the areas corresponding to the black rectangles in the mask in (a).

sample, i.e., they show intra-sample variations as well as the repeatability variations of the method. We estimate $r^2 \approx 0.88$, although it is not strictly correct to compare a visual rank order (discrete steps), with a continuously variable GAS value.

Repeatability

Each of the seven samples was measured three times. The first and the second measurements were made at the same place on the sample surface, within the accuracy of the positioning system. The second and third measurements were made on different occasions but the sample surface regions may partially overlap as each sample was appx. 20×20 mm, and the region measured was 10×10 mm. The differences between the first and second measurements thus reflect repeatability variations within the measurement device, whereas the differences between these and the third measurement also include the intra-sample variations. During a characterization of the RVM appx. 1500 positionings of the samples is necessary. This demands a high accuracy of the positioning system if two consecutive measurements are to yield similar results. Variations stem only from the inaccuracy in the positioning. The calculation of the GAS index from the RVM is purely deterministic mathematics.

Discussion

The cylindrical shaped sample holder in the measurement set-up has three important benefits. First, the shape facilitates a precise static positioning of a flexible sample surface, such as a paper surface, with a snug fit of the entire surface onto the sample holder, early realized by Pfund.[16] In Pfund's work, the main reason for using a cylinder was however that it was a convenient way of spinning the surface in order to average or low pass filter the information from the surface by making local irregularities invisible. (The cylinder approach was later abandoned[17] on the recommendation of Pfund, and the low pass filtering was instead achieved by spinning the surface on a flat circular disk.) Second, the rotating holder system facilitates changing the position

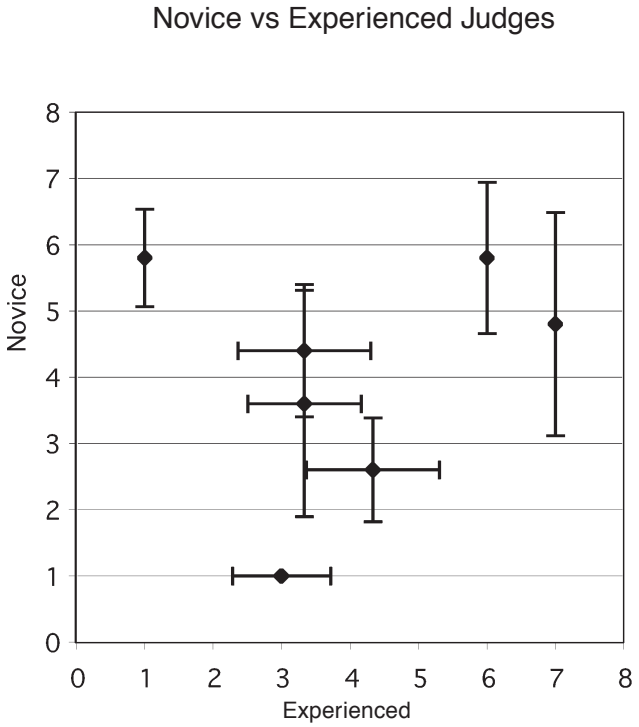

Figure 13. Results of the perceptual evaluation by the Experienced sub-group of judges plotted vs. the results of the Novice sub-group. The error bars represent the 95-percent confidence interval.

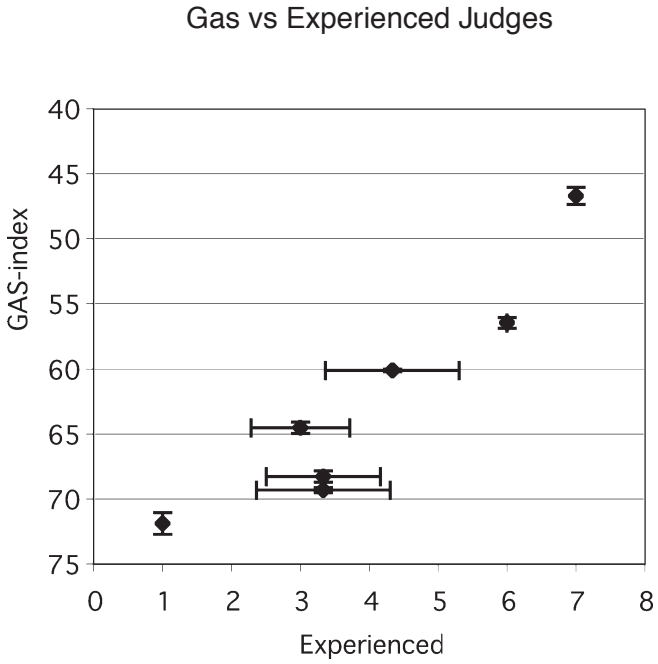

Figure 14. Results of the GAS-evaluation plotted vs. the results of the Experienced sub-group in the perceptual evaluation. The error bars represent the 95-percent confidence interval. The results and error bars for the GAS-evaluation includes measurements at different positions on each sample, i.e., intra-sample variation is included.

of the sample with a high degree of precision. Third, the holder yields a gradual shift of the sample holder inclination relative to the illumination and camera. The main difference from the goniometric approach of Arney et al,[18] is in the spatial resolution. The present method includes multiple registration of each local position (facet) under different inclinations relative to the illumination and receptor.

It is however possible to generalize the sample holder shape into whatever shape is desired for the application in question, as long as the topography of the holder is analytically described. For rigid and possibly non-flat surfaces it might be practical to discard the holder entirely and measure the sample given its inherent shape. The rotational motion of the holder may be generalized in the same manner. The transformation of the projected images of the sample into a Cartesian metric is still usually possible and the analytical description of local inclination of the holder makes the calculations similar to those presented here. The strictly convex sample holder used in this study does however have special benefits as it makes the omittance of multiple scattering and the masking of facets less severe. In the transformation from the curved projection of the sample to the flat Cartesian metric, no data are interpolated. A reasonable refinement of the transformation algorithm is to use either a linear or a more sophisticated spline interpolation, to increase the performance of the measurement.

In this study no consideration has been given to the mean gloss value. Thus we have taken a step back from the long term goal of characterizing all that is visible, by omitting the clearly visible effect of gloss level, i.e., we have here omitted what is measured in the traditional and standardized specular gloss measurement devices. In order to achieve a mean gloss value, it would be necessary to introduce a reference surface. For applications such as paper characterization, a black plastic film, e.g., a fully exposed photographic negative film, mounted on the sample holder might be suitable. Another possibility is to use a sample holder made of polished black glass, with well defined refractive index. Calibrations may then be made with samples removed from the holder. Calculations of reflectance values may be performed under these circumstances.

The CCD camera had a close to linear response in the dominate range of operation, but output levels up to approximately seven divert from a linear response. This fact does, however, have only a limited effect on the characterization algorithm, as only the peak reflectance value for each surface coordinate is stored, in which case gray scale values of less than 10 are exceptionally rare.

A limitation of the measurement strategy presented is the fixed angle between the illumination and the receptor. This imposes an inability to distinguish, e.g., among roughness effects that drastically change the reflectance characteristics for a grazing angle of illumination. For that type of surface it might prove more valuable to take the approach used by Barkas,[19] where the bisector of the illumination and receptor is fixed while the inclinations of the illumination and receptor relative to the sample surface are changed. Barkas's measurement characterizes the change of reflectance as a function of the simultaneous change of the angle of incidence and the angle of receptor.

The feature of the present analysis where the surface is inclined relative to the illumination and the judge (receptor), instead of moving the receptor in relation to

the surface and illumination, could be simulated in a goniophotometer, provided the angle between the illumination and receptor were fixed, and these were jointly moved in an arc over the sample during the measurement phase. The response curve would be similar to, but not exactly the same, as the traditional goniophotometric curve. In fact, if a measured surface had the same goniophotometric characteristics regardless of the incidence angle θ_i, the reflectance measured in the present set up as a function of the surface inclination would be identical to a normal goniophotometric curve but with twice the angular speed. However, in general, surfaces show different goniophotometric characteristics when the incidence angle θ_i is changed, with a pronounced higher degree of directed reflectance for rougher surfaces as the angle θ_i is increased.[20]

The resolution of a measuring system aimed to characterize a perceptual sensation is important. For example, considering the spatial coordinates, a matt paper surface can be perceived as homogeneous with regard to gloss and therefore of high quality, but at a low mean gloss level. The surface is however matt because it is rough on a micro-scale, a scale not resolvable by the unaided human visual system. In the present work, homogeneity is defined in relation to what is perceivable by the unaided eye. There is a natural and intrinsic distinction in the present work between how the chosen surface model treats the measured topography on different scales. On a macro scale, with dimensions well above the side length of a facet, both the directionality and level of reflection are resolved, and a *supra facet topography characterization* is achieved. On a micro scale, only the mean level of reflection is resolved, and a *sub-facet topography characterization* is obtained. The characteristics of this approach well resemble the "instrumental characteristics" of the human visual system, where the spatial resolution sets the limit of what is meant by micro and macro topography.

As the change in inclination of a local area on the sample holder take place in only one dimension, reflectance changes are also measured in only one dimension. As a consequence, facets with a tilt out of the measured plane are not measured in their maximum reflectance position. This may be a limitation of the implemented algorithm, but the results obtained resemble what is characterized by a visual inspection of the surface, if the surface is inclined in only one angular direction during inspection. The tilt angle of the facet is the inclination as it appears to a human judge under given incidence and inspection angles. It is however possible to expand the one-dimensionality in the angle descriptor of the RVM to a complete two-dimensional (2D) description. This could be done by performing two measurements of the same physical surface, with the sample rotated 90° around the surface normal axes in the second case. The two RVM's could then be merged. It is, however, not trivial to match of the two measured RVM's, rotating and translating them into an exact relative position. With a spatial resolution of 20 μm, the matching must be performed by image analysis or some other signal processing tool, not merely by manually positioning the sample on the holder. Assuming a basic reflection behavior of the facets, e.g., circularly symmetrical and monotonically decreasing reflectance from the peak reflection direction of the facet, it would be possible to prepare a complete 2D reflectance map. The result would be a locally resolved map describing both the reflectance and the two dimensional direction of facets.

In the case of the smooth plastic film, Fig. 11(a), there seems to be a correlation between the reflection and the angle map. There appear to be circular "mountains", even though the angular information is projected onto only one angular dimension. This impression may arise because the maximum reflectance measured is lower if the slopes of the surface are at unresolved angles of the measurement system, i.e., in a direction perpendicular to the slope of the sample holder, so that measured maximum reflectance for such surfaces is an underestimate of the true surface reflectance ability. This hypothesis has not, however, been tested.

The surface of the sample with an extraordinary high degree of gloss inhomogeneity, Fig. 11(c), contains many swollen fibers, clearly visible in the sample as the surface at the same time has a high mean gloss level and is perceptually very disturbing. In the RVM, the raised fibers show up as strokes of positive angles next to and appx. parallel to strokes of negative angles. These swollen fibers form "crests" over the surface.

In contrast to the sample in Fig. 11(b), both the higher amplitude and the larger spatial scales of the undulations in Fig. 11(c) can be determined by the naked eye, both in the reflectance and angle maps. In general, unless TiO_2 is used in the coating, the refractive index does not vary much over the surface, and hence topographic variations are the main cause of difference in the perception of gloss. Consequently, the ability to resolve the topography of the surface is a most important requirement in a characterization tool in the field of perception of gloss.

In the "Maple Leaf" sample, Fig. 11(d), the results indicate that the image areas are almost perfectly flat, as expected, but that the unprinted (plain paper) areas have a distribution skewed towards positive angles and on the average have a pronounced positive angle offset. This impression is further supported by Figs. 12(a)-12(d), where the imaged areas have an angle offset near zero degrees and the plain paper areas have an increasing frequency of facets for increasing (positive) angle offset over the whole range of measurement. The saturation of the angle information at ±18.7 degrees in Figs. 12(b) and 12(d) is due to the limit of the present set-up. The algorithm is designed so that a facet having an inclination at a higher angle than 18.7 degrees will be assigned the angle 18.7. Thus, even though it is not possible to know the true inclination of the facets corresponding to the rightmost bar in the histogram, it is possible to estimate the total number of facets saturated in the angle information. In Figs. 12(b) and 12(d) we can see that the rightmost bar in the histogram is indeed high, but the proportion of saturated facets is limited. The increase in facets with increasing angle offset may appear questionable but it is likely to be due to optical effects caused by topographic variations of the surface. An effect which can be called "off-specular reflectance", has been known[21,22] for centuries, where the peak reflection of an optically rough surface is in a direction with an angle larger than the angle of incidence.[20] The reflectance from a perfect diffusing surface (a Lambertian surface) does not depend on the angle of the receptor. The angle of incidence is more important and the maximum reflectance would be registered when the incidence is normal to the surface.

The angular offset effect due to the roughness of the surface is, as previously stated, well known. There is, however, a fundamental difference between the present work and the previous goniophotometric measurements. In present work there is a fixed angle between illumi-

nation and receptor whereas in the goniophotometric measurements there is a fixed position of the illumination and the surface. This slight difference should be taken into consideration when relating the results from the two different types of measurement principles. Also of importance: a high degree of off-specular effect is due to a high degree of roughness, which in turn implies a lower ability to reflect light. Hence, this type of surface area yields lower directed reflectance values. It is therefore suggested that the facets with the highest tilt angles will contribute less to the appearance of the surface than the facets with a limited tilt angle. This reasoning may motivate Fig. 12(d) to be reasonable, in spite the overall high tilt values. Note that the Figs. 12(a)-12(d) consider only the tilt information, not the corresponding directed reflectance values.

In spite of the off-specular effect of a rough surface, it would still be quite possible to construct a flaky surface almost like a tiled roof, which would yield the opposite optical behavior. However if this constructed surface were rotated 180° around the *z*-axis the flakiness would instead enhance the off-specular effect. An important question is: should this off-specular effect be measured or should it be algorithmically eliminated? If the effect is not eliminated we would normally get an offset for the mean angle value of all facets in a surface, which would be more pronounced for an unprinted surface than for a printed, glossier surface. It may be assumed that this effect is not normally perceived by a human judge, and hence not seen as a deficiency in the gloss behavior. The lack of reference direction while perceiving the reflection from a surface, cause the PA direction of reflection to be interpreted as the specular reflection, even if it is, strictly speaking, ten degrees or more off the specular direction. This suggests that the effect should be eliminated when some sort of gloss quality measure is derived. On the other hand, it might be of interest to know how large the off-specular effect actually is for a sample, and in that case the effect should not be eliminated. In this article, the only sample where the effect is not eliminated is the "Maple Leaf"-sample surface, RVM in Fig. 12(d), as the purpose was to characterize and visualize this optical effect. The choice of measuring the surface relative to the SA or the PA direction is made by performing the angular tuning phase (see *Appendix, available as Supplemental Material*) relative to the bare sample holder metal surface (SA) or relative to the sample surface to be measured (PA).

Note that the effect of the so-called "negative contrast",[23] can be observed in Fig. 11(d), where the *black* glossy imaged areas reflect more light in their local peak reflection direction than the *white* matte unprinted areas in their corresponding reflection directions.

Figures 11(d) and 12(a)-12(d) imply that it can be unwise and possibly totally misleading to make measurements on unprinted and rough surfaces with standard gloss measuring devices, which measure in the SA direction only. Standardized gloss meters would not measure the reflectance at, and at some degrees around, the direction of the PA for a rough surface. Standardized gloss meters measure more than seven degrees off the PA direction for some papers. Hence a standardized gloss meter, with an acceptance angle of only a few degrees, may, for these types of surfaces, measure mainly a bulk scattering and miss the peak reflection. Low-gloss surfaces should according to standards[24–26] be measured at a large angle (relative to the surface normal): 75°, and work by Fetsko[3] indicates that the off-specular effect for an incidence angle of 75° was about 7° for unprinted paperboard. The interpretation of Fig. 12(d) in the present work suggests that this behavior of an unprinted paper is not changed when it is measured at 20°. For smooth and glossy, possibly printed surfaces, this problem of off-specular reflectance may be negligible.

This work has also sought to develop an objective characterization algorithm for geometry dependent variations in reflection (gloss variation) that rates a surface as does a trained human judge and which can predict the result given by a panel of experienced judges. It is assumed that geometry dependent variations in reflectance intensity are important for the visual impression of the gloss quality. Instead of the more restricted "spatial variation of gloss", we here consider the more general "geometric variation of gloss". The first can be measured on a single CCD-image whereas the second requires both spatially and angularly resolved reflectometry. The geometry dependent variation in reflectance is characterized based on the RVM.

The angular coordinates of the RVM provide information about reflectance variations as a function of inclination of the sample, i.e., not as a function of inclination of the illumination *or* the receptor, as is the common characterization using a goniophotometric set up. This angular characterization resembles well the way in which an observer commonly studies a photograph or a magazine.

The RVM resolves surface undulations down to the facet dimension (*supra facet topography*), i.e., a characterization both in angle and reflectivity. The surface undulations of dimension below that of the facet are characterized only in the reflectivity (*sub facet topography*). This characteristic behavior for the instrumental spatial resolution, well resemble the behavior of the human visual system. The chosen side length of the facets, appx. 20 μm, may be a slightly higher resolution than necessary, but the signal may later be down sampled, if shown desirable. The facet approach is assumed to be a good approximation of the surface as perceived visually.

When the RVM is calculated, an attempt has been made to utilize the limited dynamics of the CCD in an effective manner by tuning the illumination to each sample individually. The drawback is that no mean gloss level can be measured or calculated, but in the perceptual evaluation, the judges were also asked to judge solely on the basis of geometry-dependent gloss variation, in an attempt to attack the multidimensionality of gloss. There is, nevertheless, more perceptual relevance in characterizing the gloss level than the homogeneity only. The long term goal is to characterize all that is visible.

The test series used in this study was challenging to evaluate, due to the small differences between the samples. The samples considered by the Experienced evaluators to be the best and worst were considered by the Novice evaluators to be No. 6 and No. 5 respectively. The difficulty of evaluating the series was, however, a desired characteristic. The results showed some variation even among the experienced judges. The results of the Novice judges gave a different overall ranking, but there was also a high degree of intra-group variation among the responses of individual judges. Perhaps the task was too difficult for the Novice judges. The correlation between the GAS index and the ratings of the experienced evaluators was fairly high.

Considering the results of the Experienced judges, we found that samples s12, s13, and s24 have similar mean rank values with little variation. This indicates that the samples where perceived to be similar. For sample s11 in relation to s12 however, the magnitude of the perceived dissimilarity cannot be assessed since there is no varia-

tion in the results for s11, which is ranked best by all the Experienced judges. The same holds true for samples s25 and s26. If we incorporate the results of the Novice panel members, it is however possible to assess the perceived appearance distances between the samples.

The RVM gives no information about the mean gloss value. It would however be possible to have a reference surface, e.g., a black plastic film on the sample holder, so that the illumination could be tuned to maintain a stabile illumination reference level. It would then be possible to extend the homogeneity measure (GAS) to include the mean gloss value of the surface.

Even omitting factors such as the MTF of the human visual system, the method has a potential to outperform Novice judges. This is suggested to be due to (a) the dimensionality of the input data, (b) the spatial and angular resolution of the measurement system, and (c) the importance of the perceptually negative component of gloss, where the negative component corresponds to disturbing glittering effects, which effectively reduce the perceived quality of surface gloss.

The encouraging results of the rather naïve and straightforward approach of the GAS evaluation may be an indication of a strength of the RVM, rather than an indication that the GAS evaluation is optimized.

It is also possible to use the RVM's and to model an illumination-observation set-up in order to simulate the reflectance behavior in a more generalized way, i.e., to simulate the dynamic reflectance behavior of a surface inclined in the desired directions controlled through an interactive computer interface.[8]

Summary

There is a close relation between the characteristics of the measurement strategy here presented and the approach often taken by a human judge, e.g., inclining and if possible flexing the sample while evaluating the gloss characteristics. This is a strong advantage and it is of fundamental importance for the explanatory potential of the proposed measurement strategy. The equipment described here is able to resolve the measured reflectance into both spatial and angular coordinates, at a resolution for these dimensions tuned to resemble approximately the corresponding resolution of a human judge, given a reasonable distance suited for a perceptual evaluation task of ca. 30 cm. The reduction of the measurement data from a large multidimensional reflection volume into the two-layer Reflection Vector Map is a condensation into a compact information set of high explanatory power, containing multiple aspects of the gloss characteristics of importance to a human judge.

The homogeneity index (GAS), though using a naïve evaluation approach, still gave encouraging results that well outperformed a panel of inexperienced judges, for the sample set studied.

Acknowledgment. The author acknowledges the financial support of the two Swedish print research programs, PFT (Print Research Program) and T2F (PrintTech Research). Special thanks are due to Per-Åke Johansson (STFI, the Swedish Pulp and Paper Research Institute STFI, Stockholm), for his supervision of the part of this work that stems from the authors Master's Thesis work. Acknowledgements are made to Staffan Rydefalk and Cathrine Östlund, (both at STFI), Petter Kolseth (Stora Enso, Falun), Björn Kruse (LiU-ITN Linköping University, Department of Science and Technology Campus Norrköping), for fruitful discussions and helpful comments and to J. Anthony Bristow for insightful suggestions on and linguistic review on this manuscript.

References

1. M. Lindstrand, Instrumental gloss characterization - In the light of visual evaluation: A review, *J. Imaging Sci. Technol.* **49,** 62 (2005).
2. V. G. W. Harrison, *Definition and measurement of gloss: a survey of published literature*, Printing and Allied Trades Research Association, Cambridge, 1945.
3. J. M. Fetsko, F. E. Witherell and G. W. Poehlein, Relationship between gloss and surface roughness of paperboard samples and prints, *Advaces in printing science and technology,* Vol. 12**,** pp. 67–72 Versailles, France, June, IPC Science and Technology Press, Guildford, UD, 1973.
4. J. M. Fetsko and A. C. Zettlemoyer, Factors affecting print gloss and uniformity, *TAPPI J.* **45**(8), 667–681 (1962).
5. A. Paul, Measuring technology for assessing gloss, *Professional Printer* **38**(2), 13–16 (1994).
6. M.-C. Béland, S. Lindberg and P.-Å. Johansson, Optical measurement and perception of gloss quality of printed matte-coated paper, *J. Pulp and Paper Sci.* **26**(3), 120–123 (2000).
7. Standard Terminology of Appearance, Standard Procedure No. E 284-99a, American Society for Testing and Materials, 1999.
8. M. Lindstrand, An interactive gloss visualization environment - For measured or simulated surface data, *J. Imaging Sci. Technol.* **47**(4), 346–356 (2003).
9. M. Lindstrand, A conceptual approach to describe gloss variation in printing paper, M.Sc. Thesis, Linköping University, 1996.
10. P.-Å. Johansson and M. Lindstrand, Swedish patent 9600816-4 (20 December 1999).
11. P.-Å. Johansson and M. Lindstrand, U.S. patent 6,147,750 (14 November 2000).
12. M. A. MacGregor and P.-Å. Johansson, Submillimeter gloss variations in coated paper. Part 1: The gloss imaging equipment and analytical techniques., *TAPPI J.* **73**(12), 161–168 (1990).
13. M. A. MacGregor and P.-Å. Johansson, Submillimeter gloss variations in coated paper. Part 2: Studying "orange peel" gloss effects in a lightweight coated paper., *TAPPI J.* **74**(1), 187–194 (1991).
14. M. A. MacGregor, P.-Å. Johansson and M.-C. Béland, Measurement of small-scale gloss variation in printed paper, *International Printing and Graphic Arts Conference*, TAPPI Press, Atlanta, GA, pp. 33-43, 1994.
15. J. A. van den Akker and G. R. Sears, Gloss of coated paper and paperboard, *TAPPI J.* **47**(11), 179A–182A (1964).
16. A. H. Pfund, The measurement of gloss, *J. Opt. Soc. Amer. & Rev. Sci. Instr.* **20**(1), 23–26 (1930).
17. G. S. Haslam and L. D. J. Grady, The Pfund glossmeter applied to paints and lacquers, *Ind. Eng. Chem. Analy., 2nd ed.* **2**(3), 346–348 (1930).
18. J. S. Arney, T. Tantalo and D. Stewart, The measurement of surface topography of materials by analysis of goniometric reflection of light: factors govering precision and accuracy, *J. Imaging Sci. Technol.* **38**(5), 489–494 (1994).
19. W. W. Barkas, A geared photometer turntable suitable for surfaces of low gloss, *J. Scientific Inst.* **19**(2), 26–29 (1942).
20. K. E. Torrance and E. M. Sparrow, Theory for off-specular reflection from roughened surfaces, *J. Opt. Soc. Amer.* **57**(9), 1105–1114 (1967).
21. P. Bouguer, *Traité d'optique sur la gradation de la lumiere (Ouvrage posthume de M. Bouguer)*, M. l'Abbé De La Caille, Paris, 1760.
22. P. Bouguer, *Optical treatise on the gradation of light* (English translation with introduction and notes by W. E. Knowles Middleton.), University of Toronto Press, Toronto, 1961.
23. M.-C. Béland and L. Mattsson, Optical print quality of coated papers, *J. Pulp and Paper Sci.* **23**(10), J493–J498 (1997).
24. Specular gloss of paper and paperboard at 75 degrees, Standard Procedure No. T 480 om-99, Technical Association of the Pulp and Paper Industry, Atlanta, GA, 1999.
25. Standard Test Method for Specular Gloss of Paper and Paperboard at 75˚, Standard Procedure No. D 1223-93, *ASTM*, 1998.
26. Paper and board. Measurement of specular gloss Part 2: 75˚ gloss with a parallel beam. DIN method, Standard Procedure No. ISO 8254-2, International Standards Organization, 1999.
27. F. W. Campbell and L. Maffei, Contrast and Spatial Frequency, *Sci. Amer.* **231**(5), 106–114 (1974).